Re-organization of Nucleolar Architecture in Myogenic Differentiation

Tetsuaki Miyake[1,2,3] and John C. McDermott[1,2,3,*]

[1]Department of Biology, York University, Toronto, ON, M3J 1P3, Canada
[2]Muscle Health Research Centre (MHRC), York University, Toronto, ON, M3J 1P3, Canada
[3]Centre for Research in Biomolecular Interactions (CRBI), York University, Toronto, ON, M3J 1P3, Canada

[*]To whom correspondence should be addressed.
Tel: +1-416-736-2100x30344; Fax: +1-416-736-5698; email: jmcderm@yorku.ca.

Keywords: Nucleolus, mTOR, myogenesis, ribosome, translation

Abstract

Myogenesis, the process of muscle differentiation, requires an extensive remodeling of the cellular transcriptome and proteome. While the transcriptional program underpinning myogenesis is well characterized, the required adaptation in protein synthesis is incompletely understood. Enhanced protein synthesis necessitates ribosome biogenesis at the nucleolus. Nucleolar size and activity are inextricably linked with altered gene expression. Here, we report changes in nucleolar morphology and function during myogenic differentiation. Immunofluorescence analysis revealed alterations in nucleolar morphology that were dependent on the cellular state: proliferative or quiescent myogenic progenitors (myoblasts or reserve cells) contain multiple small nucleoli with a characteristic spherical shape, whereas multinucleated myotubes typically contain one large, often irregularly shaped nucleolus. These morphological alterations are consistent with changes to nucleolar phase separation properties. Re-organization of the nucleolar structure was correlated with enhanced rRNA production and protein translation. Inhibition of mTOR signaling with Rapamycin perturbed nucleolar re-organization. Conversely, hyperactivated mTOR enhanced alterations in nucleolar morphology. These findings support an mTOR dependent re-organization of nucleolar structure during myogenesis, enhancing our

understanding of myogenesis and possibly facilitating new approaches to therapeutic interventions in muscle pathologies.

Introduction

The nucleolus, initially observed in the1800's, is a phase separated subnuclear compartment primarily specialized for ribosome biogenesis (Pederson, 1998). Recognition that the nucleolus exhibits dynamic changes in its architecture depending on a variety of cellular conditions has been well documented (Boulon et al., 2010). Structurally, the clustered arrays of rRNA gene repeats that are sequestered and transcribed in the FC subdomain of the tri-partite nucleolar structure arise from five distinct acrocentric chromosomes in mouse and human. Remarkably, dynamic changes in the size and fusion of nucleoli within a given interphase nucleus depend on the reorganization of multiple chromosomal regions encoding the rDNA repeats (Lafontaine et al., 2021).

Clustering the chromosomal domains encoding the rRNA genes nucleate the nucleolar organizer region (NOR) that seeds the formation of the nucleolus (Hernandez-Verdun, 2011). Actively transcribed rRNAs scaffold a variety of RNA binding proteins that often contain intrinsically disordered regions (IDRs) responsible for weak multivalent protein/protein interactions (van der Lee et al., 2014). These assemblies lead to the formation of multiphase condensates characteristic of typical nucleolar structure. The core-shell nucleolar architecture thus consists of three layers or sub-compartments: the fibrillar centre (FC); the dense fibrillar component (DFC); and the granular component (GC) (Feric et al., 2016). The FC forms the core containing rDNA repeats, transcription factors and RNA polymerase I (Pol I) for rRNA gene transcription. Nascent rRNAs are localized at the boundary between the FC and the DFC regions, and nascent rRNAs are sorted into the DFC and processed and modified by, for example, IDR containing RNA binding proteins such as Fibrillarin (Yao et al., 2019). In the outermost layer of the nucleolus, the GC, rRNAs and ribosomal proteins are assembled into rRNA/protein complexes (rRNPs) mediated by proteins such as Pescadillo and Nucleolin (Lerch-Gaggl et al., 2002; Tajrishi et al., 2011).

In proliferating cells, nucleolar formation is dynamically regulated (Hernandez-Verdun, 2006). Dissolution of the nucleolus occurs during mitosis, and the nucleolus is reassembled upon

mitotic exit (Hernandez-Verdun, 2011). At the onset of mitosis, Pol I activity ceases and the loss of nascent rRNA results in dispersion of the FC and subsequently the DFC and the GC regions in a consecutive manner (Feric et al., 2016; Yao et al., 2019). The resumption of Pol I activity after exiting mitosis triggers the re-formation of the FC region, followed by the establishment of the FC/DFC/GC multilayered structure, characteristic of the mature interphase nucleolar architecture (Dundr et al., 2000; Hernandez-Verdun, 2011; Leung et al., 2004). Therefore, alterations in the structure of the nucleolus are intrinsically linked with changes in Pol I mediated transcription of rRNA genes and ultimately to a change in the protein translational capacity of the cell (Goodfellow and Zomerdijk, 2013). Thus, modulation of nucleolar morphology under a variety of cellular states may be functionally linked to adaptations in gene expression and cellular function.

In the process of muscle cell differentiation (myogenesis), the formation of multinucleated muscle cells (myotubes (MTs)) from committed progenitor cells (myoblasts (MBs)) requires a vast orchestration of gene expression. The myogenic gene program has been a paradigm for studies on cellular differentiation since the late 1980's when the MyoD gene was first identified and characterized as a master regulatory transcription factor of the myogenic program (Davis et al., 1987; Lassar et al., 1989; Weintraub et al., 1989). Since then, the identification of other members of this basic helix-loop-helix family of sequence specific DNA binding transcription factors (sTFs), collectively termed the myogenic regulatory factors (MRFs; MyoD, Myf5, Myogenin and MRF4) have been shown to play critical roles during myogenesis (Hasty et al., 1993; Kassar-Duchossoy et al., 2004; Nabeshima et al., 1993; Rudnicki et al., 1993). Further work documented the co-operative interaction of the MRFs with members of the myocyte enhancer factor 2 (MEF2) family, forming an anciently conserved bipartite determinant of muscle specific gene transcription (Molkentin et al., 1995; Ornatsky et al., 1997). Thus, the transcriptional regulatory program underlying the production of Pol II mediated mRNA transcriptome changes orchestrating myogenesis has been well characterized. Conversely, the large changes in protein synthesis necessary to translate the altered transcriptome at the inception of differentiation into changes in the proteome leading to differentiation are less well understood (Fujita et al., 2021; Fujita et al., 2017; Zismanov et al., 2016). For example, the synthesis of large structural proteins for the bulk synthesis of sarcomeres requires substantial changes in translational control (Rommel et al., 2001).

In addition to proliferation and differentiation of myogenic cells, mature skeletal muscle fibres also possess substantial plasticity in response to a wide range of environmental and physiological demands (Egan and Zierath, 2013; Fujita and Crist, 2018). These biochemical adaptations in response to a variety of physiological cues result in adjustment of cell size and function (Fluck, 2006). For example, upon overload stimuli, muscle mass increases by hypertrophic growth mediated by an upregulation of global protein production (Bolster et al., 2003). Underlying these changes at the molecular level, activation of mammalian target of rapamycin (mTOR) kinase, which phosphorylates ribosomal S6K kinase and 4E-BP, has been implicated in activating or de-repressing translation (Battaglioni et al., 2022; Csibi et al., 2010). mTOR has also been implicated in regulating protein production by impacting ribosome biogenesis (Chaillou, 2019; Fyfe et al., 2018). Therefore, mTOR signaling appears to exert executive control over skeletal muscle mass by affecting protein translation at several levels of regulation (Coolican et al., 1997; Gugliuzza and Crist, 2022).

Consistent with the idea that changes in nucleolar morphology are linked with changes in protein translational capacity of the cell, in this study we document profound changes in nucleolar morphology during the differentiation of myogenic cells. We also document that rRNA production and protein translation are markedly upregulated during myogenesis. Congruently, repression of mTOR activity resulted in abrogation of nucleolar morphology changes and inhibition of the myogenic program. Conversely, mTOR gain of function experiments resulted in enhanced nucleolar morphology adaptations. Thus, these data implicate mTOR signaling in nucleolar morphology changes that are associated with enhanced ribosome biogenesis and protein translational capacity in differentiating myogenic cells.

Results

Re-organization of nucleolar structure in differentiating muscle cells

The inception of these studies occurred when we were visualizing nucleoli in growing and differentiating muscle cells using well characterized nucleolar marker proteins. Primarily, we observed a marked difference in the morphology of the nucleoli in that the growing proliferative myogenic progenitor cells (myoblasts; MBs) contained multiple small nucleoli with a characteristic spherical shape whereas the multinucleated differentiated cells (myotubes; MTs)

typically contained one large often irregularly shaped, nucleolus within the nucleoplasm. A previous study on the effects of creatine on myoblast differentiation also suggested a change in the myoblast nucleoli (Ohira et al., 2011). The morphology of the small spherical nucleoli is consistent with the typical archetypal phase separated nucleolus described in many previous studies (reviewed in (Lafontaine et al., 2021)). Conversely, the formation of the large, morphologically irregular shaped nucleoli observed in myotubes and their connection with nucleolar function is less well understood. The nucleolar architecture in myotubes is also less consistent with a typical liquid-liquid phase separated (LLPS) compartment in that the morphology does not have a spherical droplet shape and may involve a maturation of the biophysical properties of the nucleoli towards a gel or solid like state. This is a striking change indicating a substantial re-arrangement of genomic structure since multiple genetic loci harbor the rRNA repeats from different acrocentric chromosomes (Chromosome 12, 15, 16, 18, and 19 in mouse and Chromosome 13, 14, 15, 21, and 22 in humans) (Moss et al., 2019). In view of these novel preliminary observations, we subsequently undertook further analysis of the nucleolar changes occurring in differentiating myogenic cells.

During the differentiation program of myoblasts, many muscle restricted genes are transcribed and translated in order to form the highly specialized mature muscle cell which, among many functions, has to contract in response to membrane depolarization and also serve as a major metabolic depot in the control of metabolism. In particular, large amounts of sarcomeric proteins need to be synthesized for the formation of the contractile units, termed sarcomeres. While transcriptional control of muscle differentiation has been extensively characterized in the last forty years, the corresponding translational changes underlying this dramatic alteration of the proteome is only beginning to be understood. In view of this, we considered the possibility that the change in nucleolar structure that we observed might be crucial for enhancing ribosome biogenesis necessary to support the vast changes in protein translational capacity required for the execution of the differentiation program.

We thus hypothesized that alteration of nucleolar morphology and function is required for myotube formation. To test this idea, we initially documented the size changes of the nucleoli in differentiating and undifferentiated muscle cells. We chose the C2C12 model culture system, which has long been a well characterized model for the muscle differentiation program, to study

the nucleolar changes. These cells reliably form multinucleated differentiated MTs (MyoG+, MyHC+) after 4 days in reduced mitogenic differentiation media (DM), while under the same culture conditions, some cells within the culture become growth arrested and quiescent (Reserve cells or RCs- single nucleus / MyoG- / MyHC-). This phenomenon thus allows a direct comparison of the differentiated and undifferentiated phenotype within the same culture with clonogenic, genetically equivalent myogenic progenitor cells. To initially mark and visualize the morphology of the nucleoli, we used well-characterized antibodies that recognize nucleolar marker proteins, such as Fibrillarin (Figure 1A, Supplemental figure 1A also see Supplemental video file A&B) and Nucleolin (Supplemental figure 1B, C). Since nucleoli in MTs and RCs were not necessary located on the same optical plane, we obtained z-stacked images per one field of view and rendered one orthogonally projected image (Supplemental figure 1A, B, C). This approach allowed measurement of the size (length) of nucleoli in the MTs and RCs accurately. As seen in Figure 1A, in the MyHC+ MTs, most of the nucleoli were larger in size and less in number per nucleus compared to those of the RCs (magnified images in Figure 1B). Since Fibrillarin forms clusters of small foci at the DFC phase of the nucleolus, we also stained for Nucleolin, which localizes to the GC layer (the outermost region of the tri-partite multiphase nucleolus), to confirm that the nucleoli observed in the MTs was a continuous GC layer (Figure 1C and Supplemental figure 1D, E). To clearly identify the nucleolus in the nucleus in two different cellular states in the same field of view, we used MyoG staining as a marker for the differentiating cells to distinguish the multinucleated MTs from the mono-nucleated RCs (Figure 1D and Supplemental figure 1F&G). We also extended the analysis to proliferating myoblasts (MBs) in growth media (GM) (Figure 1E). Comparison of the average nucleolar size (average length of nucleoli) in MBs, MTs and RCs was 2.35 ± 1.33μm (n=225), 4.11 ± 3.18μm (n=97), and 1.43 ± 0.54μm (n=480) respectively. Of the three distinguishable populations (MBs, MTs, and RCs) the MTs exhibited enhanced nucleolar size and less nucleoli compared to both the RCs ($p<0.00001$) and the MBs ($p<0.0001$). To carefully document the nucleolar size distribution in each cell state, we sorted the nucleoli into 5 categories based on their length (Figure 1F). These data verify an increasing percentage of the large nucleoli (>4.5μm) in differentiating cells compared to the RCs (Figure 1F). Since the C2C12 cell line was originally isolated from clonal colonies derived from mouse leg muscle (Yaffe and Saxel, 1977) we wanted to determine if the nucleolar changes we documented in C2C12 are also observed in primary mouse skeletal muscle

satellite cells. To do this we utilized myoblasts derived from mouse hindlimb skeletal muscle satellite cells isolated from gastrocnemius and tibialis anterior muscles. Similar alterations in nucleolar morphology and size were observed in primary mouse skeletal myocytes (Figure 2A, B).

In summary, under differentiation conditions, the size and number of nucleoli were markedly different depending on the cellular differentiation status in both C2C12 cells and primary mouse skeletal muscle myoblasts (satellite cells). In contrast to these observations in myogenic cells, no significant morphological size changes occurred in the nucleoli of fibroblast cell lines (C3H10T1/2, and NIH3T3), when the cells were exposed to DM conditions ($p>0.05$) (Supplemental figure 2), indicating that the nucleolar changes are a function of the myogenic differentiation program and not a general cellular response to the differentiation conditions.

Nucleolar activity during myogenic differentiation

It has been reported that generally, there is a positive correlation between the size and biosynthetic activity of the nucleolus. Since we observed large nucleoli in the differentiated MTs and smaller, more abundant ones in the RCs, we postulated that the nucleolar activity might be enhanced in the MTs compared to the RCs. To test this idea, we took advantage of the fact that the majority (>85%) of RNAs in a cell are rRNAs produced in the nucleolus (Kraus et al., 2019). We therefore used an RNA specific fluorescent dye (SytoRNA Select) to stain accumulated RNAs using a live-cell imaging technique. The rationale being that the majority of RNA signal is generated from rRNA biogenesis, and indeed nucleoli were marked by this RNA dye (Figure 3A). Remarkably the signal intensity of SytoRNA Select was apparently higher in the MTs than in the RCs within the same cultures (Figure 3B). Quantification of signal intensity by 2.5 intensity plot analysis (Figure 3B) and a line scan (Figure 3C) of Hoechst (DNA) and SytoRNA Select signals indicates that signal intensity was considerably higher in the MTs (green open arrows) than in the undifferentiated RCs (red open arrows). We further converted the intensity of the fluorescence signal derived from SytoRNA Select to a Heat Map (HM) to visualize the overall level of RNAs in the different cellular states, and similar to the observations described above, MTs had higher signal intensity than RCs (Figure 3D). To confirm that the enhanced

overall RNA production in the MTs leads to an upregulation of translational capacity, puromycin was added into the media to label nascently synthesized polypeptides. The cells were then fixed and subjected to IF analysis for quantification of active translation by means of visualization of puromycylated peptide accumulation (Figure 3E). In addition, the translational capacity indicated by puromycin incorporation was linked with the morphology of the nucleoli by Nucleolin staining, and for MT formation by F-actin accumulation (Figure 3E). Substantially higher accumulation of puromycylated peptides was observed in the MTs compared to the RCs, confirming a higher translational capacity in tandem with the large increase in rRNA and the changes in nucleolar structure observed. Altogether, global translational activity is higher in differentiating cells and lower in the cells maintaining an undifferentiated state even under the same low mitogen culture conditions. These data collectively infer that there is a dramatic and regulated induction of rRNA biogenesis and protein translation in differentiating myogenic cells that is correlated with nucleolar morphology changes.

mTOR activity regulates the size of nucleoli and is required for muscle differentiation

Based on the possibility, alluded to above, that a cellular program is invoked to promote nucleolar re-organization and rRNA biogenesis in differentiating myogenic cells, we noted that the mTOR signaling pathway has been previously implicated as an important regulator of nucleolar function in a variety of cellular contexts (reviewed in (Battaglioni et al., 2022)). Therefore, to test if mTOR might play a similar role in myocytes, we initially inhibited mTOR activity using the well characterized cell-permeable pharmacological inhibitor, Rapamycin, and recorded the morphology of the nucleoli (a working model is outlined in Figure 4A). We confirmed that components of the canonical mTOR signaling pathway such as S6K and UBF, a key transcription factor involved in rRNA gene transcription, are expressed in myogenic cells (Figure 4B). The levels of two nucleolar proteins, Nucleolin and Fibrillarin, were upregulated when the cells were exposed to DM and maintained during the differentiation program (after DM2). In addition, we monitored the cellular localization of P-S6K (S389) (Figure 4C) and total S6K (Figure 4D) in MTs and RCs (DM4) by IF analysis. We noted that the active, phosphorylated form of S6K (P-S6K) accumulated in the nuclei of both MTs and RCs, while the

signal intensity of P-S6K was higher in differentiating cells (MyHC+) depicted by the HM (Figure 4E).

Next, we examined if mTOR inhibition by Rapamycin treatment impacts the nucleolar morphology. To assess this, C2C12 cells were maintained in DM for 4 days with or without Rapamycin (Figure 5A). First, in the control condition, in agreement with previous results, the average size of nucleoli in the MyHC+ cells (MTs) was larger than that of the MyHC- cells ($p<0.00001$), and the average size of nucleoli in the nucleus of MyHC+ cells treated with Rapamycin was almost identical to that of the nucleoli in MyHC- cells (Figure 5B). Thus, it appears that the nucleolar size changes observed in the differentiation time course are essentially negated by Rapamycin treatment. In addition, we observed that 70.0% of the cellular nuclei were in MyHC+ cells (MTs) in DM, whereas in the presence of Rapamycin, it was reduced to 20.4% (Figure 5C) indicating that the differentiation program was also inhibited. In addition, in contrast to the control condition where most MyHC+ cells are multinucleated, most if not all MyHC+ cells in Rapamycin treated cultures were mono-nucleated. Thus, Rapamycin inhibited both the enlargement of the nucleoli and also subsequent MT formation. In order to ascertain whether the loss of nucleolar re-organization in Rapamycin treated cells was a secondary effect of inhibiting the onset of differentiation we added Rapamycin to the cultures after 2 days in DM (Figure 5E). We reasoned that this would allow the cells to initiate differentiation and concomitantly allow us to see if nucleolar re-organization is still inhibited. At day2 in DM, C2C12 cells started forming multinucleated MTs. At day4, control cells differentiated to form MTs (MyHC+) (Figure 5D), and the size of nucleoli were significantly larger than that of RCs (MyHC-) (Figure 5F). In the presence of Rapamycin, multinucleated MTs were formed but the size of nucleoli was almost identical to that of the RCs indicating that Rapamycin inhibited the nucleolar re-organization even in differentiating cells. In agreement with cellular morphology, 80.6% of the cellular nuclei were in MyHC+ cells (MTs) in DM, whereas in the presence of Rapamycin, it was reduced to 58.8% (Figure 5G). We further substantiated these findings by analysis at an earlier time point (DM2) using MyoG as a differentiation marker (Supplemental figure 3A, B, C). These data suggest an integral role of mTOR signaling in nucleolar re-organization and function that is to some degree, independent of the differentiation program. Based on these data, we propose that nucleolar re-organization is a property of myogenic cells that is not secondary to the differentiation program.

mTOR gain of function enhances nucleolar size

Since the loss of mTOR kinase activity reported above resulted in the loss of enlarged nucleoli found in differentiating cells, we next used a gain of function approach to further address the mechanistic role of mTOR signaling in nucleolar changes. To do this we employed gain of function mutations of the mTOR kinase which result in hyperactivation of its kinase activity. Exogenous expression of mTOR1 S2215Y, mTOR1 I2500F, or empty vector (pcDNA3) was carried out by transient transfection into C2C12 MBs, and transfected cells were marked by expression of a co-transfected GFP expression vector (Figure 6). Whereas the size of nucleoli in GFP+ and GFP- (non-transfected) cells in the pcDNA3 control group (GFP+ (n=116) / GFP- (n=254) = 1.11 ± 1.07) were not significantly different, the average area of the nucleoli in mTOR1 S2215Y, and I2500F expressing cells (GFP+) was, on average, 2.87 ± 3.24 (GFP+ (n=82) / GFP- (n=226) and 3.50 ± 3.68 (GFP+ (n=73) / GFP- (n=407) times larger than those of non-transfected cells (GFP-) ($p<0.00001$). Thus, both gain (mTOR1 S2215Y and I2500F) and loss (Rapamycin) of function studies indicate a key role of mTOR signaling in nucleolar re-organization in myogenic differentiation.

Collectively, we document novel observations indicating a dramatic mTOR dependent re-organization of nucleoli in differentiating myogenic cells that may underpin substantial changes in ribosomal RNA production and protein translation capacity during muscle cell differentiation.

Discussion

The Nucleolus is a critical phase separated sub-nuclear compartment that subserves gene expression by functioning as a factory for rRNA transcription and initial steps in ribosome biogenesis. In this study, we document profound changes in nucleolar morphology during the program of myogenic differentiation. Re-organization of nucleolar structure is correlated with a dramatic enhancement of rRNA production and a concomitant increase in protein translation. Further studies employing gain and loss of function strategies revealed that perturbing nucleolar re-organization impedes the myogenic differentiation program. Specifically, we observed that Rapamycin treatment, which has been previously characterised as preventing nucleolar size changes by inhibiting mTOR, prevents both nucleolar re-organization and myogenic

differentiation. Conversely, gain of function experiments using a hyperactive mTOR mutation promotes nucleolar enlargement in myogenic cells, which is a signature of increased rRNA production and protein translational capacity. Manipulation of mTOR signaling did not alter nucleolar morphology in non-myogenic cells suggesting it may be a unique requirement for differentiating muscle cells. These studies document that mTOR signaling regulates an important re-organization of nucleolar structure and function that is required for myogenic differentiation. These novel findings may facilitate new avenues of discovery for therapeutic intervention in muscle pathologies such as rhabdomyosarcoma and sarcopenia and in muscle regeneration following injury.

mTOR signaling in nucleolar function

Ribosome biogenesis is one of the most energy consuming cellular processes as > 85% of cellular RNA is composed of rRNAs (Kraus et al., 2019), underscoring why the nucleolus is so fundamental to cellular function. In particular, differentiation into specialized cells requires a massive re-arrangement of gene expression to facilitate the differentiation specific cellular proteome. Historically, the ribosome was considered as a non-specialized part of the cellular "house-keeping" machinery; however, recent reports highlight the heterogeneity of ribosome composition in differentiated cells. For example, ribosomal protein large 3-like (*rpl3l*) is exclusively expressed in striated muscles and its expression is diminished during hypertrophic growth (Chaillou et al., 2016). Therefore, although it has been well-established that transcriptional control of mRNA encoding genes is a primary event for both cellular differentiation and functional muscle adaptations, efficient protein synthesis due to selective translation of mRNAs by specialized ribosomes might also prove important, therefore highlighting why a more complete understanding of nucleolar function, rRNA transcription and ribosome biogenesis are imperative. Further characterization of the mTOR signalling pathway and its role in nucleolar organization and activity during myogenesis is thus warranted.

In the model of *in vitro* muscle differentiation employed here, undifferentiated reserve cells (RCs) and differentiating cells (MTs) are remarkably derived from genetically equivalent clonogenic myoblasts within the same culture. One feature of this bi-partite cell fate decision is that the nucleolar activity and organization of the nucleolus in the two cell states are

diametrically opposed. In MTs, the nucleoli are highly active in rRNA production, morphologically enhanced in size and non-spherical. In RCs, the nucleoli exhibit low levels of rRNA production and are morphologically spherical, small, and numerous compared to those in MTs. In agreement with other reports, there is an established causal relationship between the size of the nucleolus and its activity (Buchwalter and Hetzer, 2017; Neumuller et al., 2013); MTs have active and larger nucleoli and RCs conversely have inactive and smaller nucleoli within the same culture conditions. In conditions of hypertrophic growth, a downstream effector of the mTOR kinase, S6K, which is activated by phosphorylation at T389 (P-S6K), accumulates in the MT nuclei (Bouquier et al., 2020). In agreement with this, we also observed a selective accumulation of P-S6K in the MT nuclei, suggesting the possibility that mTOR signaling may play an important role in nucleolar re-organization in muscle differentiation and adaptation.

Changes in nucleolus morphology during myogenesis

Changes in nucleolar morphology in differentiating myocytes prompted us to consider the underlying biophysical phenomena leading to such alterations. Since it is well established that the nucleolus is one of the archetypal membrane-less liquid-liquid phase separated (LLPS) compartments in the cell, we considered whether the changes observed might be due to modulation of the phase separation properties of the nucleolus. While the biophysical basis of different phase separated compartments is quite complex and requires rigorous analysis, we can clearly observe that the typical LLPS spherical nucleoli seen in the undifferentiated RC and myoblast cells gives way to a much larger and non-spherical morphology in the differentiated MTs consistent with an alteration in the nucleolar phase properties. This could be due to a transition or “maturation” from a liquid to a gel or solid like state that has been well documented in the phase separation literature (reviewed in (Lafontaine et al., 2021)). Moreover, we recently documented that c-Jun targeting to the nucleoli in myogenic cells can lead to a similar change in the nucleolar morphology in myogenic cells (Miyake and McDermott, 2022). The key question now concerns whether the changes observed in morphology are causally linked with alterations in nucleolar function. Preliminary correlative data suggests that this may be the case and this question needs further interrogation. The field of phase separation as it relates to biological

systems is still in its infancy but promises to provide definitive tools and knowledge to answer these important questions related to nucleolar morphology and function.

In summary, we have documented substantive re-organization of the nucleolar morphology in differentiating myogenic cells. This property is conserved in primary satellite cells from mouse hindlimb muscle. Nucleolar re-organization is correlated with a dramatic induction of cellular RNA synthesis and protein translation. Characterization of the assembly and maturation of the phase separated properties of the nucleolus will no doubt further our understanding of the global changes in RNA and protein synthesis leading to myogenic differentiation. Moreover, these new insights concerning nucleolar function may spawn new therapeutic approaches to various muscle pathologies and muscle regeneration.

Materials and Methods

Cell culture

C2C12 myoblasts (CRL-1772), C3H10T1/2 (CCL-226), and NIH/3T3 (CRL-1658) cells were obtained from the American Type Culture Collection. Cells were maintained in growth media (GM) consisting of Dulbecco's modified Eagle's medium (DMEM: D6429, MilliporeSigma) and supplemented with 10% fetal bovine serum (HyClone) and 1% penicillin-streptomycin (516106, MilliporeSigma) in a moisturized incubator (Model 3120, ThermoFisher) at 5% CO_2 and 37°C. Myotube formation was induced by transferring C2C12 cells to differentiation medium (DM, DMEM with 2% FBS) upon reaching 80-90% confluency. Primary mouse skeletal muscle satellite cells were obtained from iXCells Biotechnologies (10MU-033). These cells are derived from mouse skeletal muscle satellite cells isolated from mouse hindlimb gastrocnemius and tibialis anterior muscles.

The cells were thawed according to the manufacturer's protocol and directly plated on glass-bottom dishes (ibidi). The cells were maintained in GM (DMEM+20%FBS) and differentiation was initiated at 70-80% confluency in DM (DMEM+2%FBS) for 4 days.

Antibodies and Reagents

α P-S389-S6K (B2H9L3: #701064) was obtained from ThermoFisher. α Nucleolin (D4C7O: #14574) or (E5M7K: #87792) were obtained from Cell Signaling technology. α MyoG (F5D), α MyHC (MF20), and α puromycin (PMY-2A4) were obtained from Developmental Studies Hybridoma Bank (The University of Iowa, Department of Biology, Iowa City, IA 52242). α S6K (H-9: sc-8418), α CKM (C-14: sc-15164), and α β-Actin (I-19, sc1616) was obtained from Santa Cruz. α P-S484-UBF (EPR2725(2): ab182583) and α Fibrillarin (38F3: ab4566) were obtained from Abcam. For immunoblotting, HRP-conjugated secondary antibodies were obtained from MilliporeSigma (goat α-rabbit; #1662408, goat α-mouse; #1721011). For immunofluorescence, Alexa Fluor 488 or 546 conjugated antibodies were obtained from ThermoFisher (goat α-rabbit AF-488: A-11070, goat α-rabbit AF-546: A-11035, goat α-mouse AF-546: A-11030).

SYTO RNASelect Green Fluorescent cell Stain (5mM solution in DMSO: #s32703), CellMask Deep Red Plasma membrane Stain (C10046), and Hoechst 33342 Solution (20mM: 62249) were obtained from ThermoFisher. Rapamycin (#9904) was obtained from Cell Signaling. Puromycin dihydrochloride (PUR333) were obtained from BioShop.

Immunofluorescence analysis

C2C12 cells were seeded on polymer-coated glass-bottom dishes (#81158, ibidi) and fixed with 4% paraformaldehyde (PFA) in phosphate buffer saline (PBS: P3813, MilliporeSigma) on ice for 5 mins and for 10 mins at room temperature. To remove PFA, cells were washed 3X with PBS and permeabilized with ice-cold 90% Me-OH for 1 min on ice. Cells were washed again 3X with PBS and incubated with blocking buffer (5% FBS in PBS) for 2 h at room temperature, and then incubated with the indicated primary antibodies in blocking buffer overnight at 4^0C. After 3X washes with PBS to remove the unbound primary antibody, cells were incubated with appropriate Alexa fluor conjugated secondary antibody in the blocking buffer at room temperature for 1.5 h. After 3X washes with PBS, the cells were counter stained with Hoechst 33342 (B2261-25MG, MilliporeSigma) and subjected to confocal fluorescent imaging with a Zeiss Observer Z1 microscope equipped with a Yokogawa CSU-X1 spinning disk equipped with 100X objective lens (α Plan-APOCHROMAT 100X NA1.46 Oil DIC(UV) VIS-IR, 420792-

9800, Zeiss). Images were recorded by AxioCam MRm camera (Zeiss) or Evolve camera (electron-multiplying CCD camera: Teledyne Photometrics) and processed using Zen 2.5 (blue edition) software (Zeiss).

Live-cell imaging

Cells were seeded on polymer-coated glass-bottom dishes (#81158, Ibidi) and transfected with indicated expression plasmids. Next day, the cell culture media was replaced with FluoBrite (A1896701, ThermoFisher) supplemented with 10%FBS (HyClone) for imaging. During imaging, the cells were maintained in a moisturized environmental chamber (5% CO_2) at 37°C on the confocal fluorescence microscope (Zeiss Observer Z1). For staining of RNAs, SYTO RNASelect (S32703, ThermoFisher) was added to the cell culture media to a final concentration of 5μM. For membrane staining, CellMask Deep Red (C10046, ThermoFisher) was added according to the manufacturer's protocol. Images were recorded using an Evolve camera (electron-multiplying CCD camera: Teledyne Photometrics) or AxioCam MRm camera (Zeiss) and processed using Zen 2.5 (blue edition) software (Zeiss).

Image processing

Orthogonal maximum projection images and 3D-rendering images were generated from Z-stack images obtained at 240nm intervals using Zen 2.5 (blue edition) software (Zeiss). Length of nucleolus was measured on the orthogonal projection images using Zen 2.5 (blue edition) software (Zeiss). The size of nucleoli was also determined on the threshold orthogonal projection images using Analyze Particles/ImageJ (National Institutes of Health Image).

Immunoblotting analysis

Cells were harvested after 3X washes with PBS. Spun down cells were lysed with constant agitation at 4°C for 30min and total cellular proteins were extracted with NP-40 lysis buffer (NP-40 (1% (vol/vol)), 50 mM Tris-HCl (pH 8), 150 mM NaCl, and 5 mM EDTA (pH 8), 1 mM sodium orthovanadate, 10mM sodium fluoride, and supplemented with protease inhibitor

cocktail (P-8340, MilliporeSigma). Protein concentrations were determined by standard Bradford assay. Equivalent amounts of protein were boiled in sodium dodecyl sulfate (SDS) loading buffer (100 mM Tris-HCL (pH 6.5), 200 mM DTT, 4%(weight/vol) SDS, 3mM bromophenol blue, and 15% (weight/vol) glycerol) for 5min and then separated in SDS-polyacrylamide gels (SDS-PAGE) by electrophoresis with PageRuler prestained protein ladder (#26616, ThermoFisher). The proteins separated were transferred to immobilon-FL polyvinylidene difluoride (PVDF) membrane (IPFL00010, MilliporeSigma) from SDS-PAGE according to the manufacturer's instructions. The membrane was blocked with blocking buffer (5% skim-milk in PBS) prior to incubation with primary antibody at 4°C overnight with agitation. After 3X washes with PBS, appropriate HRP-conjugated secondary antibody was added and incubated for 2 h at room temperature. After washing 3X with PBS, the protein/antibody immuno-complexes were detected by a chemical reaction with Enhanced Chemiluminescence (ECL) substrate (WBLUC0500, MilliporeSigma) and recorded using an iBright CL1500 imaging system (ThermoFisher). The images were processed using iBright software (ThermoFisher).

Puromycin incorporation Assay

Puromycin was added to the media (final concentration to 0.5μM) and maintained for 15 mins in the cell culture incubator. The cells were washed 3X with PBS and fixed and permeabilized and subjected to IF analysis with α puromycin antibody (PMY-2A4).

Transfections

For ectopic protein expression, cells were transfected with a mixture of Lipofectamine 2000 (#11668027, ThermoFisher) and indicated mammalian expression DNA constructs diluted with Opti-MEM (#31985062, ThermoFisher) according to the manufacturer's protocol.

Plasmids

Mammalian expression constructs for pcDNA3-FLAG-mTOR-S2215Y (Addgene #69013) and pcDNA3-FLAG-mTOR-I2500F (Addgene #69014) was a gift from David Sabatini (Addgene #69013) (Grabiner et al., 2014).

Nucleolar size measurement

Length of nucleoli of MBs, MTs, and RCs on the orthogonal projection images was measured using Zen software. Size (area) of nucleoli of cells on the orthogonal projection images was measured using ImageJ. The average size (area) and the standard deviation were calculated and average FI of the size of nucleoli in each condition was analysed by One-way ANOVA and Tukey's HSD pairwise comparisons within the ANOVA data.

Acknowledgements

JCM is funded by research grants from the Canadian Institutes of Health Research (CIHR, project grant no PJT-159644) and the Natural Sciences and Engineering Research Council of Canada (NSERC, Discovery grant no RGPIN-2018-05896). JCM is supported by the McLaughlin Research Chair in the Faculty of Science, York University.

References

Battaglioni, S., Benjamin, D., Walchli, M., Maier, T. and Hall, M. N. (2022). mTOR substrate phosphorylation in growth control. *Cell* **185**, 1814-1836.

Bolster, D. R., Kimball, S. R. and Jefferson, L. S. (2003). Translational control mechanisms modulate skeletal muscle gene expression during hypertrophy. *Exerc Sport Sci Rev* **31**, 111-6.

Boulon, S., Westman, B. J., Hutten, S., Boisvert, F. M. and Lamond, A. I. (2010). The nucleolus under stress. *Mol Cell* **40**, 216-27.

Bouquier, N., Moutin, E., Tintignac, L. A., Reverbel, A., Jublanc, E., Sinnreich, M., Chastagnier, Y., Averous, J., Fafournoux, P., Verpelli, C. et al. (2020). AIMTOR, a BRET biosensor for live imaging, reveals subcellular mTOR signaling and dysfunctions. *BMC Biol* **18**, 81.

Buchwalter, A. and Hetzer, M. W. (2017). Nucleolar expansion and elevated protein translation in premature aging. *Nat Commun* **8**, 328.

Chaillou, T. (2019). Ribosome specialization and its potential role in the control of protein translation and skeletal muscle size. *J Appl Physiol (1985)* **127**, 599-607.

Chaillou, T., Zhang, X. and McCarthy, J. J. (2016). Expression of Muscle-Specific Ribosomal Protein L3-Like Impairs Myotube Growth. *J Cell Physiol* **231**, 1894-902.

Coolican, S. A., Samuel, D. S., Ewton, D. Z., McWade, F. J. and Florini, J. R. (1997). The mitogenic and myogenic actions of insulin-like growth factors utilize distinct signaling pathways. *J Biol Chem* **272**, 6653-62.

Csibi, A., Cornille, K., Leibovitch, M. P., Poupon, A., Tintignac, L. A., Sanchez, A. M. and Leibovitch, S. A. (2010). The translation regulatory subunit eIF3f controls the kinase-dependent mTOR signaling required for muscle differentiation and hypertrophy in mouse. *PLoS One* **5**, e8994.

Davis, R. L., Weintraub, H. and Lassar, A. B. (1987). Expression of a single transfected cDNA converts fibroblasts to myoblasts. *Cell* **51**, 987-1000.

Dundr, M., Misteli, T. and Olson, M. O. (2000). The dynamics of postmitotic reassembly of the nucleolus. *J Cell Biol* **150**, 433-46.

Egan, B. and Zierath, J. R. (2013). Exercise metabolism and the molecular regulation of skeletal muscle adaptation. *Cell Metab* **17**, 162-84.

Feric, M., Vaidya, N., Harmon, T. S., Mitrea, D. M., Zhu, L., Richardson, T. M., Kriwacki, R. W., Pappu, R. V. and Brangwynne, C. P. (2016). Coexisting Liquid Phases Underlie Nucleolar Subcompartments. *Cell* **165**, 1686-1697.

Fluck, M. (2006). Functional, structural and molecular plasticity of mammalian skeletal muscle in response to exercise stimuli. *J Exp Biol* **209**, 2239-48.

Fujita, R. and Crist, C. (2018). Translational Control of the Myogenic Program in Developing, Regenerating, and Diseased Skeletal Muscle. *Curr Top Dev Biol* **126**, 67-98.

Fujita, R., Jamet, S., Lean, G., Cheng, H. C. M., Hebert, S., Kleinman, C. L. and Crist, C. (2021). Satellite cell expansion is mediated by P-eIF2alpha-dependent Tacc3 translation. *Development* **148**.

Fujita, R., Zismanov, V., Jacob, J. M., Jamet, S., Asiev, K. and Crist, C. (2017). Fragile X mental retardation protein regulates skeletal muscle stem cell activity by regulating the stability of Myf5 mRNA. *Skelet Muscle* **7**, 18.

Fyfe, J. J., Bishop, D. J., Bartlett, J. D., Hanson, E. D., Anderson, M. J., Garnham, A. P. and Stepto, N. K. (2018). Enhanced skeletal muscle ribosome biogenesis, yet attenuated mTORC1 and ribosome biogenesis-related signalling, following short-term concurrent versus single-mode resistance training. *Sci Rep* **8**, 560.

Goodfellow, S. J. and Zomerdijk, J. C. (2013). Basic mechanisms in RNA polymerase I transcription of the ribosomal RNA genes. *Subcell Biochem* **61**, 211-36.

Grabiner, B. C., Nardi, V., Birsoy, K., Possemato, R., Shen, K., Sinha, S., Jordan, A., Beck, A. H. and Sabatini, D. M. (2014). A diverse array of cancer-associated MTOR mutations are hyperactivating and can predict rapamycin sensitivity. *Cancer Discov* **4**, 554-63.

Gugliuzza, M. V. and Crist, C. (2022). Muscle stem cell adaptations to cellular and environmental stress. *Skelet Muscle* **12**, 5.

Hasty, P., Bradley, A., Morris, J. H., Edmondson, D. G., Venuti, J. M., Olson, E. N. and Klein, W. H. (1993). Muscle deficiency and neonatal death in mice with a targeted mutation in the myogenin gene. *Nature* **364**, 501-6.

Hernandez-Verdun, D. (2006). Nucleolus: from structure to dynamics. *Histochem Cell Biol* **125**, 127-37.

Hernandez-Verdun, D. (2011). Assembly and disassembly of the nucleolus during the cell cycle. *Nucleus* **2**, 189-94.

Kassar-Duchossoy, L., Gayraud-Morel, B., Gomes, D., Rocancourt, D., Buckingham, M., Shinin, V. and Tajbakhsh, S. (2004). Mrf4 determines skeletal muscle identity in Myf5:Myod double-mutant mice. *Nature* **431**, 466-71.

Kraus, A. J., Brink, B. G. and Siegel, T. N. (2019). Efficient and specific oligo-based depletion of rRNA. *Sci Rep* **9**, 12281.

Lafontaine, D. L. J., Riback, J. A., Bascetin, R. and Brangwynne, C. P. (2021). The nucleolus as a multiphase liquid condensate. *Nat Rev Mol Cell Biol* **22**, 165-182.

Lassar, A. B., Buskin, J. N., Lockshon, D., Davis, R. L., Apone, S., Hauschka, S. D. and Weintraub, H. (1989). MyoD is a sequence-specific DNA binding protein requiring a region of myc homology to bind to the muscle creatine kinase enhancer. *Cell* **58**, 823-31.

Lerch-Gaggl, A., Haque, J., Li, J., Ning, G., Traktman, P. and Duncan, S. A. (2002). Pescadillo is essential for nucleolar assembly, ribosome biogenesis, and mammalian cell proliferation. *J Biol Chem* **277**, 45347-55.

Leung, A. K., Gerlich, D., Miller, G., Lyon, C., Lam, Y. W., Lleres, D., Daigle, N., Zomerdijk, J., Ellenberg, J. and Lamond, A. I. (2004). Quantitative kinetic analysis of nucleolar breakdown and reassembly during mitosis in live human cells. *J Cell Biol* **166**, 787-800.

Miyake, T. and McDermott, J. C. (2022). Nucleolar localization of c-Jun. *FEBS J* **289**, 748-765.

Molkentin, J. D., Black, B. L., Martin, J. F. and Olson, E. N. (1995). Cooperative activation of muscle gene expression by MEF2 and myogenic bHLH proteins. *Cell* **83**, 1125-36.

Moss, T., Mars, J. C., Tremblay, M. G. and Sabourin-Felix, M. (2019). The chromatin landscape of the ribosomal RNA genes in mouse and human. *Chromosome Res* **27**, 31-40.

Nabeshima, Y., Hanaoka, K., Hayasaka, M., Esumi, E., Li, S., Nonaka, I. and Nabeshima, Y. (1993). Myogenin gene disruption results in perinatal lethality because of severe muscle defect. *Nature* **364**, 532-5.

Neumuller, R. A., Gross, T., Samsonova, A. A., Vinayagam, A., Buckner, M., Founk, K., Hu, Y., Sharifpoor, S., Rosebrock, A. P., Andrews, B. et al. (2013). Conserved regulators of nucleolar size revealed by global phenotypic analyses. *Sci Signal* **6**, ra70.

Ohira, Y., Matsuoka, Y., Kawano, F., Ogura, A., Higo, Y., Ohira, T., Terada, M., Oke, Y. and Nakai, N. (2011). Effects of creatine and its analog, beta-guanidinopropionic acid, on the differentiation of and nucleoli in myoblasts. *Biosci Biotechnol Biochem* **75**, 1085-9.

Ornatsky, O. I., Andreucci, J. J. and McDermott, J. C. (1997). A dominant-negative form of transcription factor MEF2 inhibits myogenesis. *J Biol Chem* **272**, 33271-8.

Pederson, T. (1998). The plurifunctional nucleolus. *Nucleic Acids Res* **26**, 3871-6.

Rommel, C., Bodine, S. C., Clarke, B. A., Rossman, R., Nunez, L., Stitt, T. N., Yancopoulos, G. D. and Glass, D. J. (2001). Mediation of IGF-1-induced skeletal myotube hypertrophy by PI(3)K/Akt/mTOR and PI(3)K/Akt/GSK3 pathways. *Nat Cell Biol* **3**, 1009-13.

Rudnicki, M. A., Schnegelsberg, P. N., Stead, R. H., Braun, T., Arnold, H. H. and Jaenisch, R. (1993). MyoD or Myf-5 is required for the formation of skeletal muscle. *Cell* **75**, 1351-9.

Tajrishi, M. M., Tuteja, R. and Tuteja, N. (2011). Nucleolin: The most abundant multifunctional phosphoprotein of nucleolus. *Commun Integr Biol* **4**, 267-75.

van der Lee, R., Buljan, M., Lang, B., Weatheritt, R. J., Daughdrill, G. W., Dunker, A. K., Fuxreiter, M., Gough, J., Gsponer, J., Jones, D. T. et al. (2014). Classification of intrinsically disordered regions and proteins. *Chem Rev* **114**, 6589-631.

Weintraub, H., Tapscott, S. J., Davis, R. L., Thayer, M. J., Adam, M. A., Lassar, A. B. and Miller, A. D. (1989). Activation of muscle-specific genes in pigment, nerve, fat, liver, and fibroblast cell lines by forced expression of MyoD. *Proc Natl Acad Sci U S A* **86**, 5434-8.

Yaffe, D. and Saxel, O. (1977). Serial passaging and differentiation of myogenic cells isolated from dystrophic mouse muscle. *Nature* **270**, 725-7.

Yao, R. W., Xu, G., Wang, Y., Shan, L., Luan, P. F., Wang, Y., Wu, M., Yang, L. Z., Xing, Y. H., Yang, L. et al. (2019). Nascent Pre-rRNA Sorting via Phase Separation Drives the Assembly of Dense Fibrillar Components in the Human Nucleolus. *Mol Cell* **76**, 767-783 e11.

Zismanov, V., Chichkov, V., Colangelo, V., Jamet, S., Wang, S., Syme, A., Koromilas, A. E. and Crist, C. (2016). Phosphorylation of eIF2alpha Is a Translational Control Mechanism Regulating Muscle Stem Cell Quiescence and Self-Renewal. *Cell Stem Cell* **18**, 79-90.

Figures

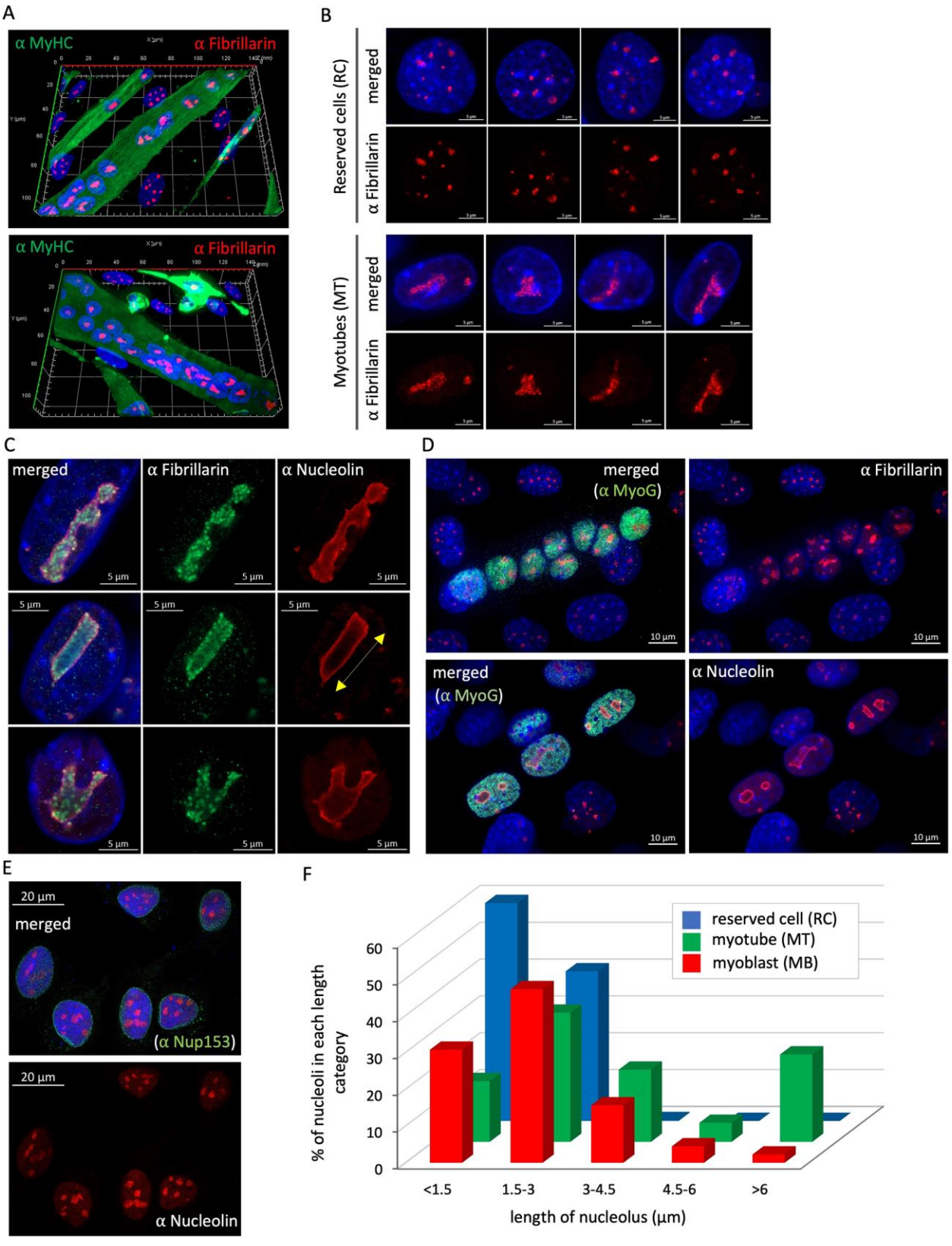

Fig. 1. Re-organization of nucleolar structure in differentiating muscle cells.

Myogenic cells (C2C12) were maintained in DM for 4 days and then fixed and subjected to IF analysis. Differentiated multinucleated MTs were marked by MyHC (green) and distinguished from undifferentiated RCs (MyHC-). Nucleolar morphology was visualized by Fibrillarin staining (red). The nucleus (blue) was stained using Hoechst 33342. (A) Z-stack images were obtained at 240nm interval by confocal microscopy. 3D-images from the Z-stacks images were rendered using Zen software. (B) Magnified orthogonal projection images of nucleoli from RCs (upper panel) and MTs (lower panel). Fibrillarin (red) depicted nucleolar morphology. (C) Magnified orthogonal projection images of nucleoli from MTs. Nucleolar morphology was visualized using Fibrillarin (green) and Nucleolin (red) staining. An example measurement of the nucleolar length is indicated by the yellow double-head arrow. (D) Nucleoli of the MTs were marked by MyoG staining (green). Nucleolar morphology was visualized by Fibrillarin (red: upper panel) and Nucleolin (red: lower panel) staining on orthogonal projection images. (E) Proliferating C2C12 cells maintained in GM were fixed and stained by Hoechst 33342 (nucleus: blue), Nup153 (green), and Nucleolin (red). (F) Length of nucleoli on the orthogonal projection images of MBs (n=225), MTs (n=97), and RCs (n=480) was measured using Zen software. Nucleoli were categorized according to their length (1.5μm intervals). % of each category over total was calculated and graphed.

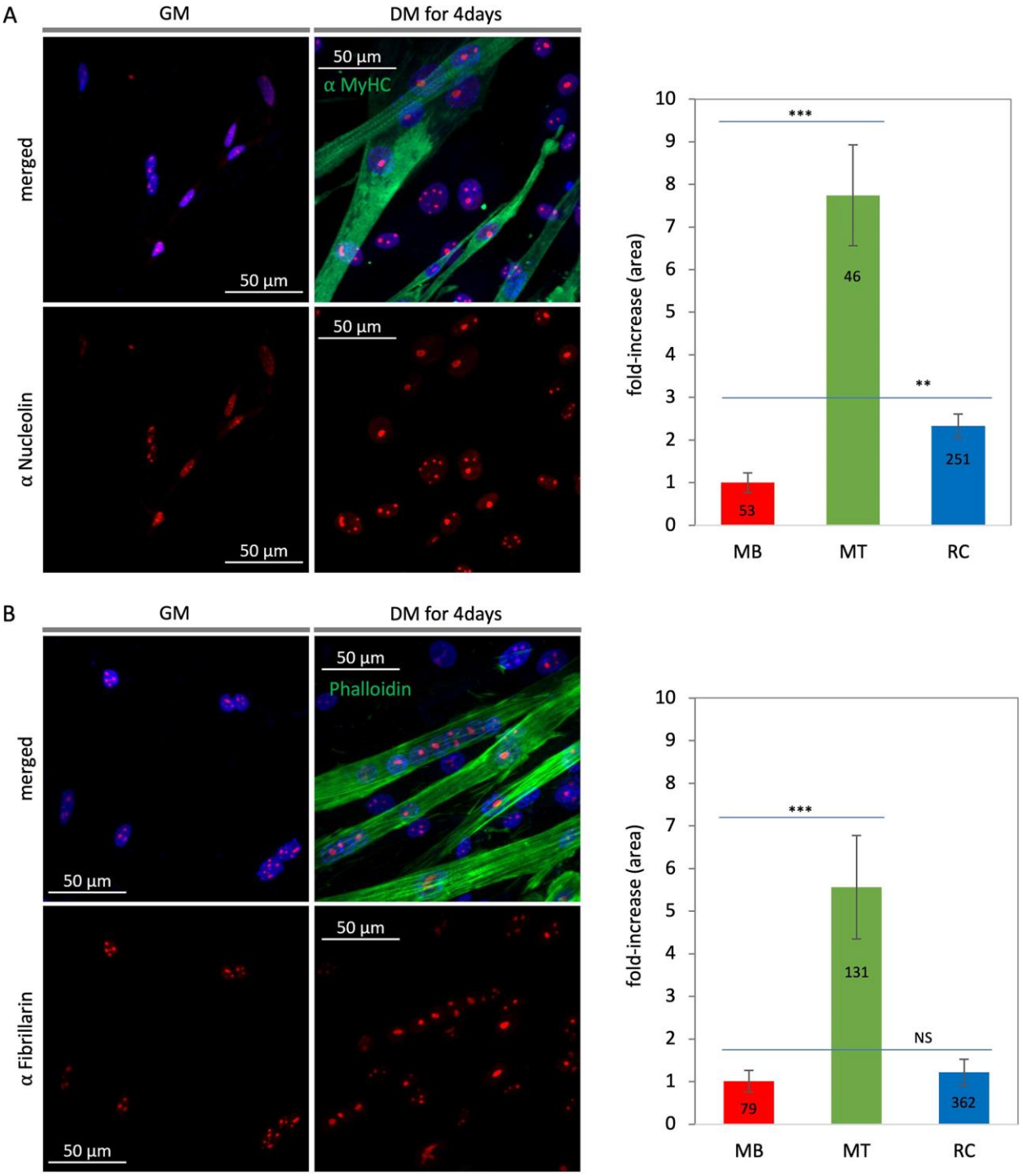

Fig. 2. Nucleolar re-organization in satellite cells from mouse hindlimb muscle.

Mouse skeletal myoblasts (satellite cells) derived from mouse hindlimb gastrocnemius and tibialis anterior muscles were seeded onto glass-bottom dishes with GM (20% FBS). Upon

growth to high density, the cells were transferred to DM (2% FBS) and maintained for 4 days. The cells were fixed and subjected to IF analysis for Nucleolin (red)/MyHC (green) (A) or Fibrillarin (red) /F-actin (green) (B). The nuclei were stained by Hoechst 33342 (Blue). Z-stack images (240nm intervals) were obtained by confocal fluorescence microscopy, and orthogonal projection images were generated using Zen software (Zeiss). The size of each nucleolus was measured using ImageJ software. Fold-increases (area) were calculated relative to the average size of the nuclei in the MBs and graphed, error bars represent standard deviations. Numbers on the bar graph indicate the number of nucleolar measurements. The significance of the difference between samples was tested by One-way ANOVA (NS: not significant ($P>0.05$), **: $P<0.001$, ***: $P<0.0001$). MB= in myoblast, MT=in myotubes, RC=in reserve cells.

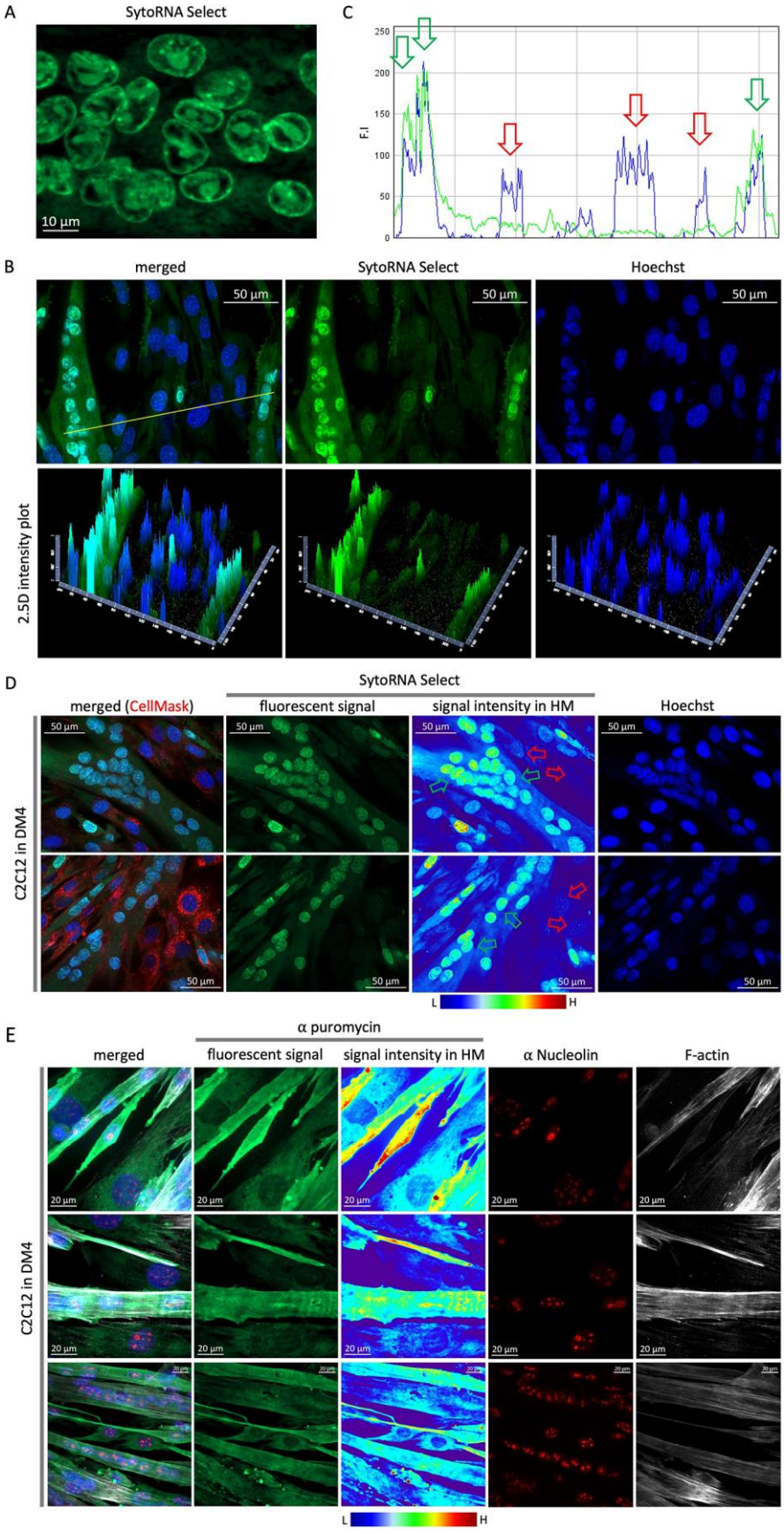

Fig. 3. Nucleolar activity during myogenic differentiation.

Myogenic Cells (C2C12) were maintained in DM for 4 days. (A) Magnified micrograph of nuclei in the MT stained by SytoRNA Select. (B) Hoechst 33342 (blue) and SytoRNA Select (green) were added to the media, and the cells were subjected to live cell imaging. Z-stack images (240nm intervals) were obtained by confocal fluorescence microscopy, and orthogonal projection images were generated using Zen software. Signal intensity of SytoRNA Select and Hoechst were shown in the 2.5D intensity plot generated by Zen software. (C) In addition, a line scanning analysis of the fluorescence intensity on the yellow line was shown on the graph. Position of corresponding to MT or RC are indicated green or red open arrows. (D) A signal intensity of SytoRNA Select and Hoechst was converted to a Heat Map (HM). MTs and reserved cells are marked by green open arrows and red open arrows respectively. (E) Cells maintained in DM for 4 days were subjected to Puromycin labeling. Puromycin was added into the media (final concentration of 0.5μM) for 15 min. The cells were fixed, puromycylated peptides (green) and Nucleolin (red) were detected by IF technique with corresponding antibodies. Nuclei (blue) and F-actin (white) were counterstained with Hoechst 33342 and phalloidin AF-633 respectively. Z-stack images (240nm intervals) were obtained using confocal fluorescence microscopy, and orthogonal projection images were generated by Zen software. Signal intensity of puromycin incorporation was converted to a Heat Map (HM).

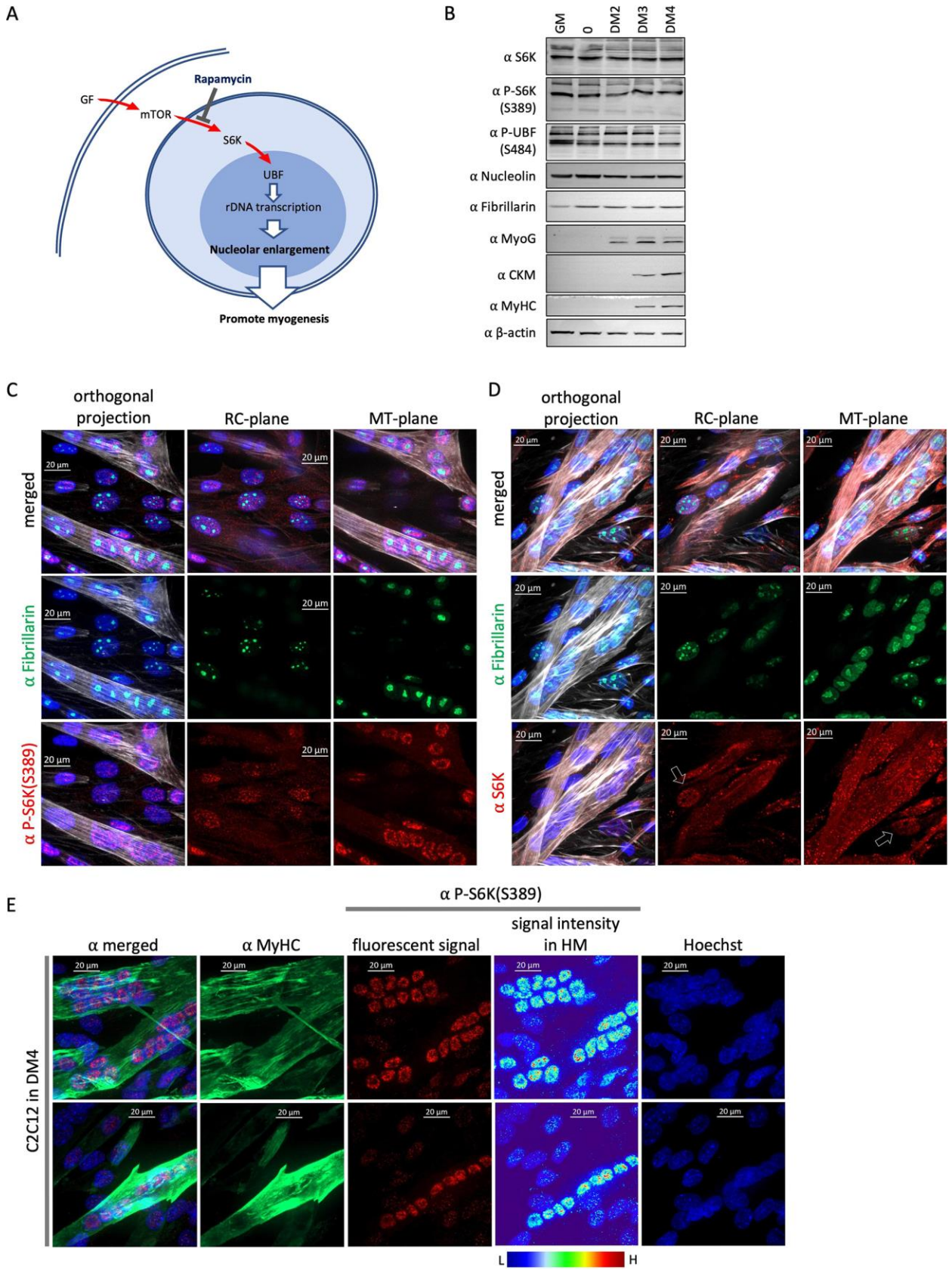

Fig. 4. mTOR activity regulates the size of nucleoli and is required for muscle differentiation.

(A) schematic working model of involvement of mTOR pathway in nucleolar function. (B) C2C12 cells were seeded and harvested as indicated. Total cell lysate was subjected to immunoblotting analysis. Expression levels of indicated proteins were detected by corresponding antibodies and visualized with ECL-conjugated secondary antibody. β-actin levels served as loading control. (C) Cells maintained in DM for 4 days were fixed and subjected to IF analysis for Fibrillarin (green) and P-S6K (S389) (red), and counter-stained for nuclei (blue) and F-actin (white) with Hoechst 33342 and phalloidin AF-633, respectively. Z-stack images (240nm intervals) were obtained by confocal fluorescence microscopy, and orthogonal projection images (left hand side panel), and single optical plane (MT-plane or RC-plane) were generated using Zen software. (D) Duplicated conditions as in C above with IF analysis for total S6K (red). Nuclear localization was indicated by open arrows. (E) The orthogonal projection image of P-S6K(S389) in C was converted to a Heat Map (HM) based on the signal intensity. MyHC marks MTs.

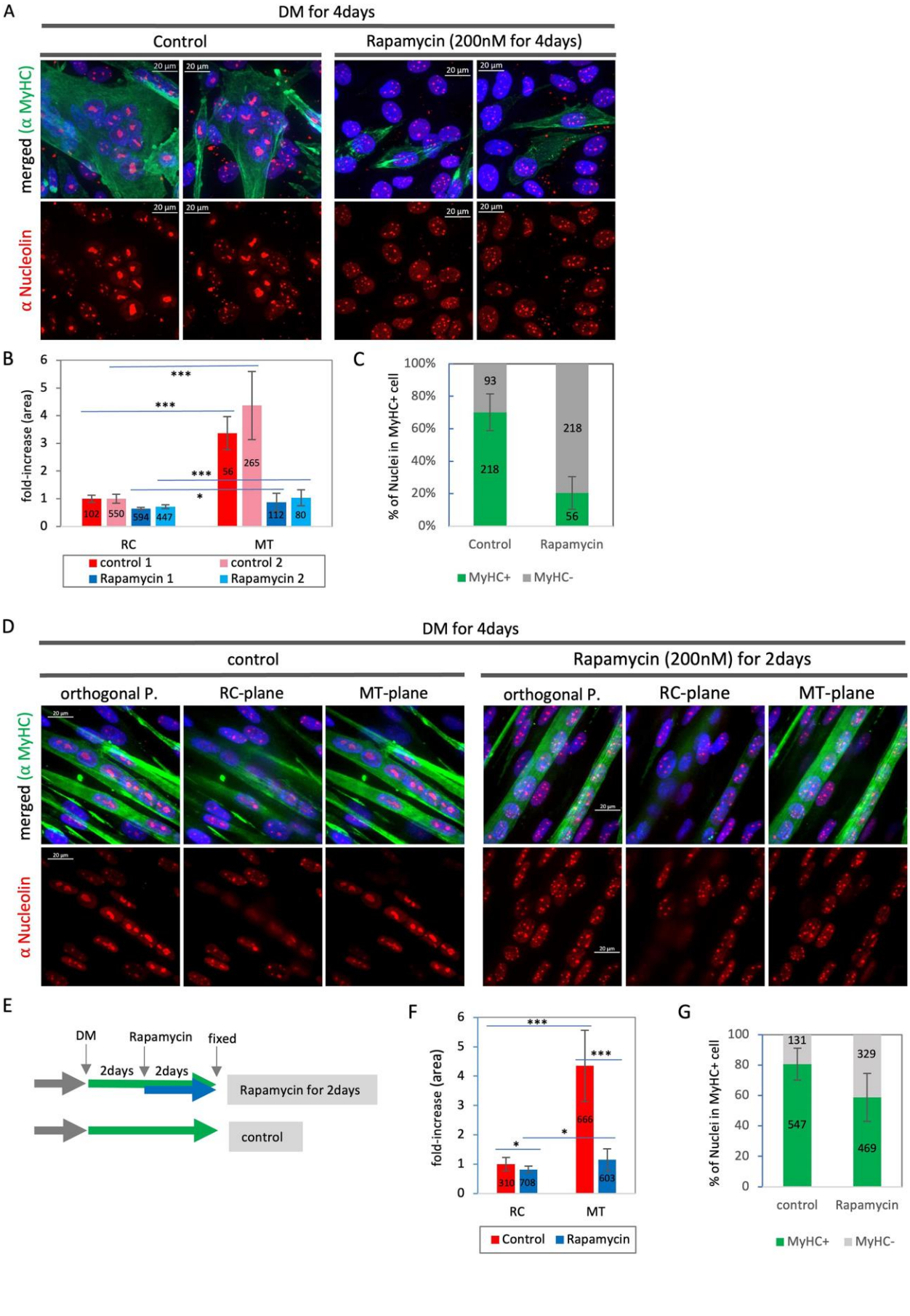

Fig. 5. Inhibition of mTOR signaling by Rapamycin blunted myogenesis and rearrangement of nucleolar morphology.

Under differentiation conditions, myoblasts were treated with Rapamycin or solvent control for 4days in DM (A, B, and C) or 2days in DM for 4days (D, E, F, and G). (A and D) The cells were fixed and subjected to IF analysis for MyHC (green) and Nucleolin (red) and counterstained for nuclei with Hoechst 33342 (blue). Z-stack images (240nm intervals) were obtained by confocal fluorescence microscopy, and orthogonal projection images were generated by Zen software. (B and F) The size (area) of nucleoli in MyHC+ cells and MyHC- cells on the orthogonal projection images (3 to13) of control (n=2) and Rapamycin (n=2) treated cells were measured using ImageJ. Average sizes were graphed, and error bars represent standard deviations among the measurements. Numbers on the bar graph indicate number of the measurements. The significance of the difference between samples was tested by One-way ANOVA (*: $p<0.05$, **: $P<0.001$, ***: $P<0.0001$). (C and G) Number of nuclei in MyHC+ cells and MyHC- cells were counted using more than 9 (13 to 22) micrographs in each condition and % was calculated and graphed. Error bar represents standard deviations among the samples. Numbers on the bar graph indicate number of the measurements. (E) A schematic of the experimental design.

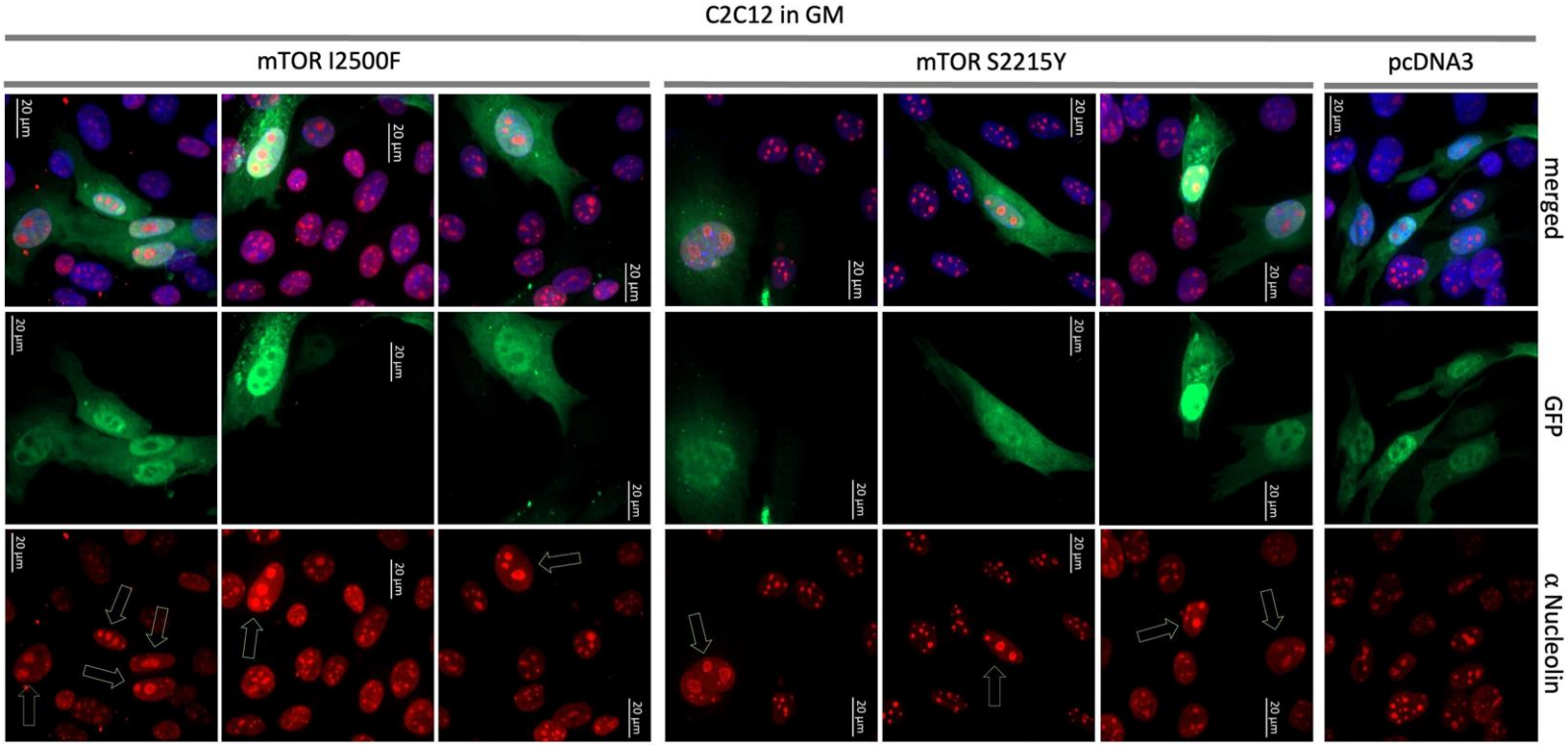
C2C12 in GM
mTOR I2500F
mTOR S2215Y
pcDNA3
merged
GFP
α Nucleolin
20 µm

Fig. 6. mTOR gain of function enhances nucleolar size.

Myogenic cells (C2C12) were transfected with pcDNA3, mTOR S2215Y or mTOR I2500F expression vector and GFP expression vector for monitoring transfection. (A) The cells were fixed and subjected to IF analysis for Nucleolin (red) and Fibrillarin (white, not shown) and counterstained for nuclei with Hoechst 33342 (blue). Z-stack images (240nm intervals) were obtained by confocal fluorescence microscopy and orthogonal projection images were generated by Zen software. Open green arrows indicate GFP+ (transfected) cells.

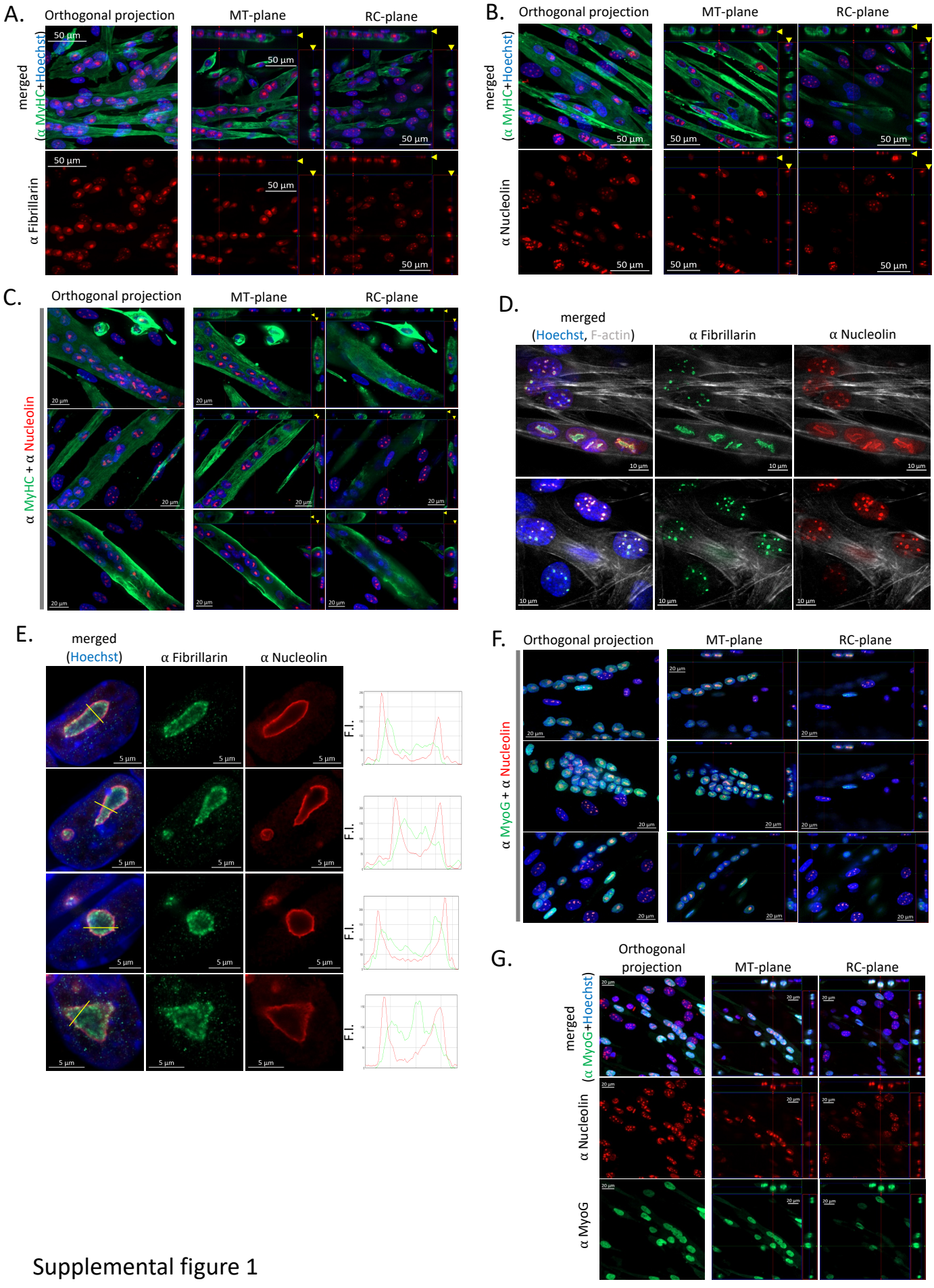

Supplemental figure 1

Fig. S1. Re-organization of nucleolar structure in differentiating muscle cells.

C2C12 cells were seeded onto the glass-bottom dishes in DM for 4 days. The cells were fixed and subjected to IF analysis. Differentiated multinucleated MTs were marked by MyHC (green) and distinguished from undifferentiated RCs (MyHC-). Their nucleolar morphology was visualized by Fibrillarin (A: red) or Nucleolin (B and C: red). Nuclei (blue) were stained with Hoechst 33342. Z-stack images were obtained at 240nm interval by confocal microscopy. Orthogonal projection images were generated from the Z-stacks images by Zen software. MT-plane and RC-plane were derived from optical slices from the Z-stacks in the MTs (MyHC+) or RCs (MyHC-), respectively. (D) IF analysis of Fibrillarin (green) and Nucleolin (red) in the MTs and RCs at DM4. The cells were counterstained for nuclei and F-actin by Hoechst 33342 and phalloidin AF-633, respectively. Micrographs were orthogonal projection images. (E) Magnified images of nuclei of the MTs in DM4. Nucleoli were visualized using Fibrillarin (red) and Nucleolin (green) staining by IF technique. Fibrillarin and Nucleolin represented DFC and GC regions of the nucleolus respectively. Line scanning analysis for green (Fibrillarin) and red (Nucleolin) signal on the yellow line depicted sub-nucleolar localization of Fibrillarin (DFC) and Nucleolin (GC). (F and G) Differentiating C2C12 cells for 4days in DM (F) or for 2 days in DM (G) were marked by IF analysis for MyoG (green, and their corresponding nucleolar morphology was visualized by Nucleolin (red). The cell nucleus was stained with Hoechst 33342.

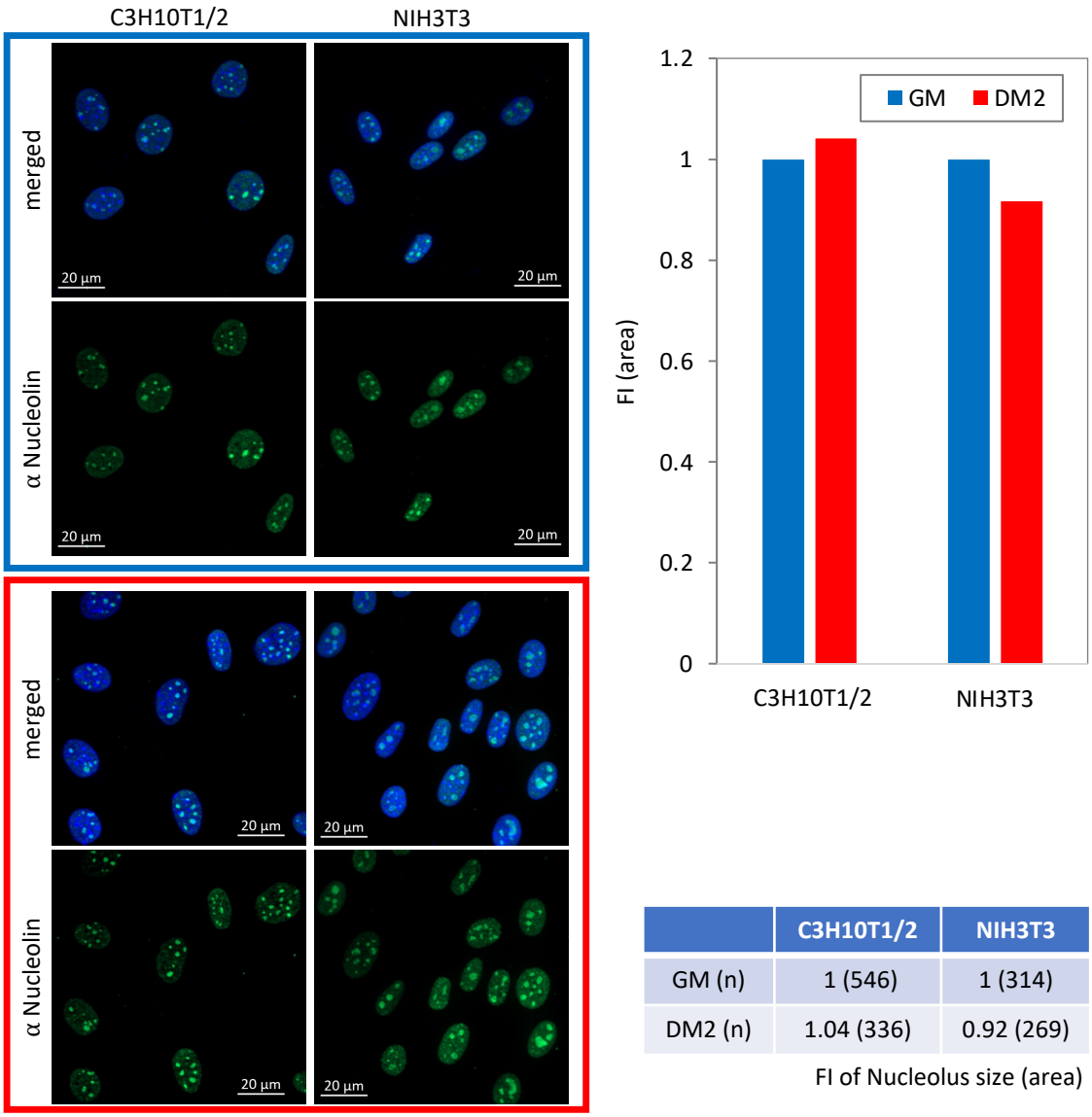

	C3H10T1/2	NIH3T3
GM (n)	1 (546)	1 (314)
DM2 (n)	1.04 (336)	0.92 (269)

FI of Nucleolus size (area)

Fig. S2. No obvious re-organization of nucleolar structure in non-muscle cells in DM

C3H10T1/2 and NIH3T3 cells were seeded onto glass-bottom dishes. The cells were fixed in GM or in DM conditions for 2 days. Nucleoli were visualized by Nucleolin (green), and the nuclei were counterstained with Hoechst 33342 (blue). Z-stack images (240nm intervals) were obtained by confocal fluorescence microscopy, and orthogonal projection images were generated by Zen software. The area of the nucleolus on the threshold orthogonal projection images of GM (blue square) and DM2 of C3H10T1/2 and NIH3T3 were measured by Analyze Particle function of ImageJ software. Average size of the nucleoli at DM2 was calculated relative to the average size of the GM. The average of the fold-increase (FI) of the relative size of the DM2 (red bar) to the GM (blue bar) was graphed. Values were shown in the table. One-way ANOVA indicates that differences between nucleolus size in C3H10T1/2 in GM and DM2, NIH3T3 in GM and DM are not significantly different at $p<0.05$ ($p=0.564277$ and $p=0.392786$ respectively).

A.

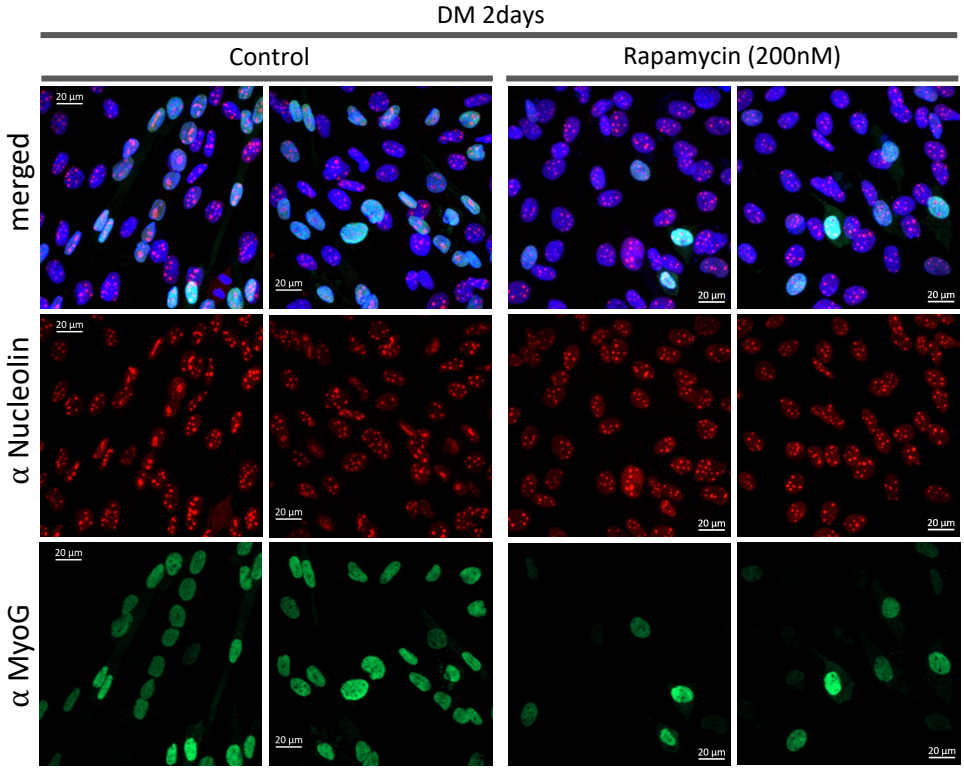

B.

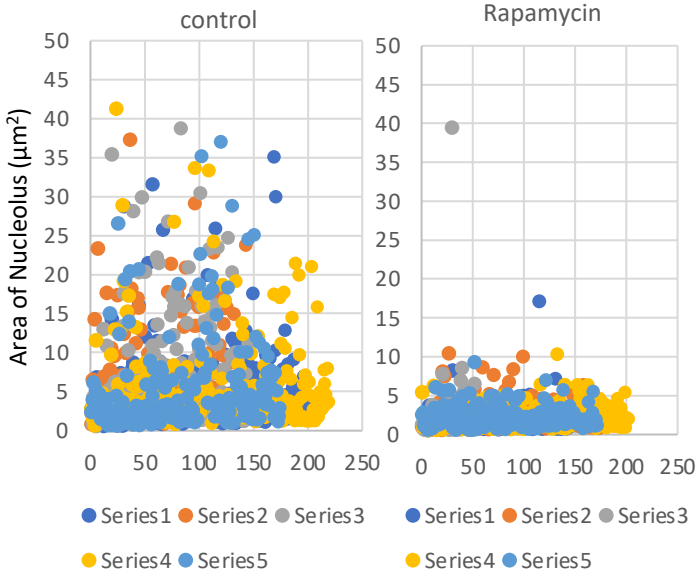

(n)	Area (ave.)
Control (958)	6.28
Rapamycin (858)	2.25

C.

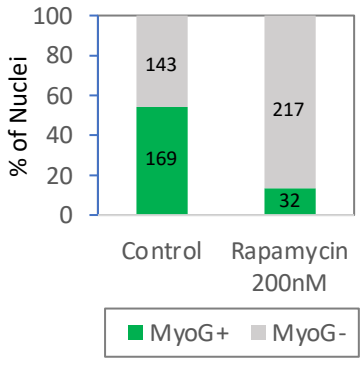

Supplemental figure 3

Fig. S3. mTOR activity regulates the size of nucleoli and is required for muscle differentiation.

(A) C2C12 cells were seeded onto glass-bottom dishes and the cells were transferred to DM in the presence of Rapamycin (200nM) or its solvent and maintained for 2 days. The cells were fixed and subjected to IF analysis. Differentiating cells were marked by MyoG (green). Their nucleolar morphology was visualized by Nucleolin (red). Nuclei (blue) were stained by Hoechst 33342 (blue). Z-stack images were obtained at 240nm intervals by confocal microscopy. Orthogonal projection images were generated from the Z-stack images by Zen software. (B) Using 5-threshold images each to determine the area of each nucleolus by Analyze Particle function of ImageJ software and graphed. An average size of the nucleoli with or without rapamycin was calculated and shown in the table. One-way ANOVA indicates that the difference between control and Rapamycin is significant at $p<0.00001$. (C) % of MyoG+ nuclei were calculated and graphed (control: 54.2%, Rapamycin: 13.4%). Actual numbers are shown on the bar in the graph.

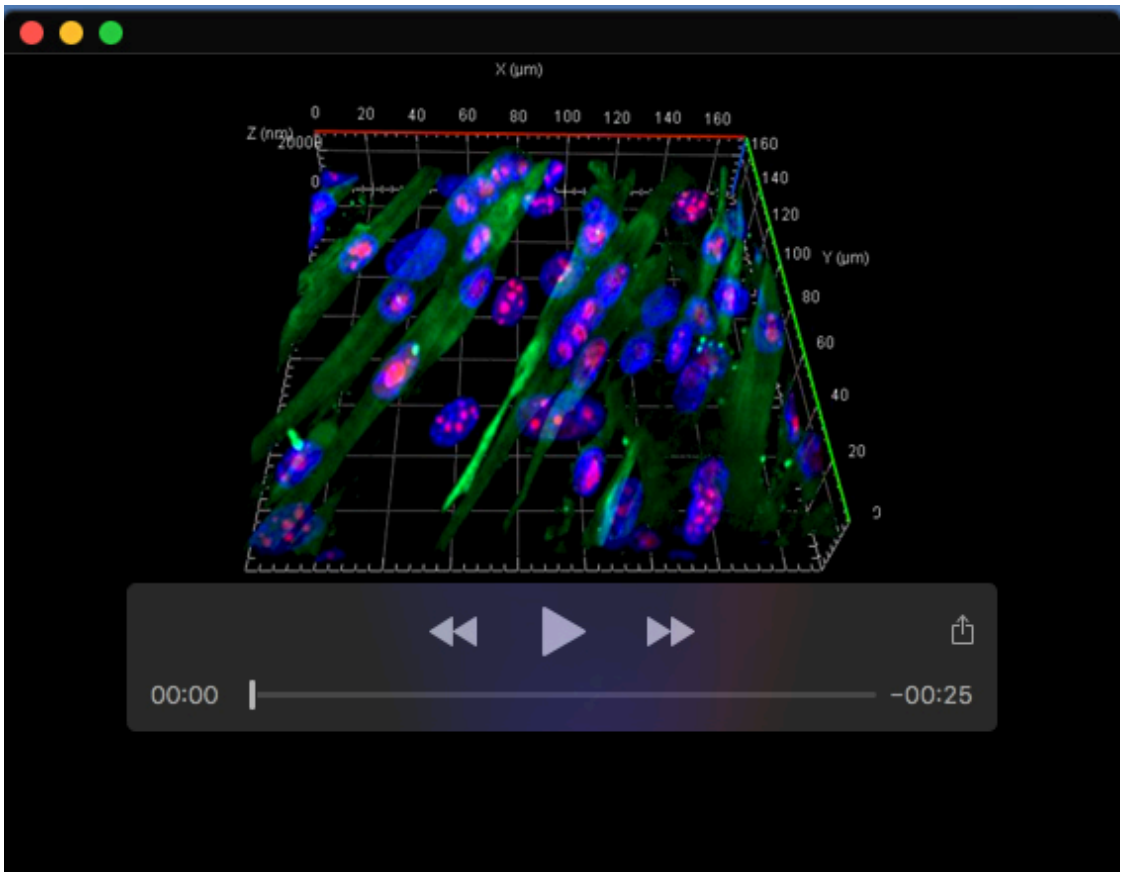

Movie 1. C2C12 cells were seeded onto the glass-bottom dishes and cells were transferred to DM and maintained for 4 days. The cells were fixed and subjected to IF analysis. Differentiated multinucleated MTs were marked by MyHC (green). Their nucleolar morphology was visualized by (A) Nucleolin (red) or (B) Fibrillarin (red). Nucleus (blue) was stained by Hoechst 33342. Z-stack images were obtained at 240nm interval by a confocal microscopy technique. 3D-images from the Z-stacks images were rendered by Zen software.

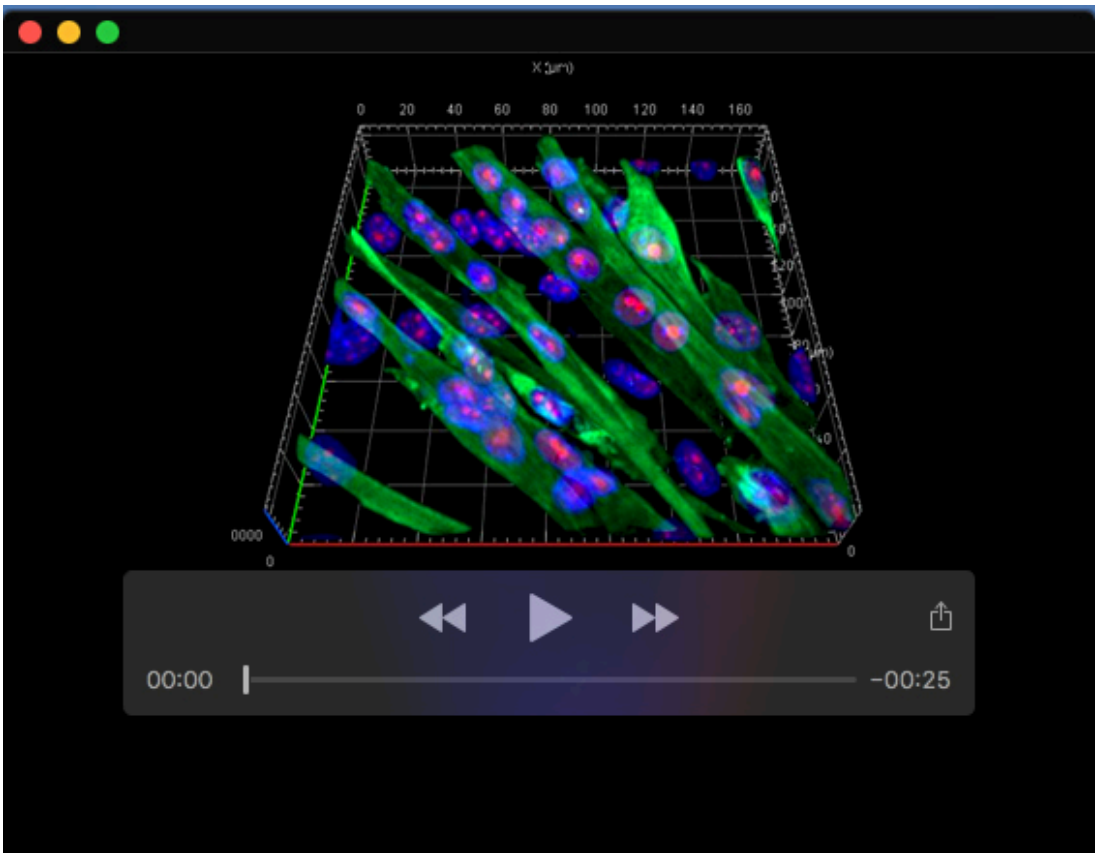

Movie 2. C2C12 cells were seeded onto the glass-bottom dishes and cells were transferred to DM and maintained for 4 days. The cells were fixed and subjected to IF analysis. Differentiated multinucleated MTs were marked by MyHC (green). Their nucleolar morphology was visualized by (A) Nucleolin (red) or (B) Fibrillarin (red). Nucleus (blue) was stained by Hoechst 33342. Z-stack images were obtained at 240nm interval by a confocal microscopy technique. 3D-images from the Z-stacks images were rendered by Zen software.

Journal of Cell Science • Supplementary information